



## Fabrication of MoS<sub>2</sub>-Graphene Nanocomposites by Layer-by-Layer Manipulation for High-Performance Lithium Ion Battery Anodes

Yuhai Hu,<sup>a,\*</sup> Xifei Li,<sup>a</sup> Andrew Lushington,<sup>a</sup> Mei Cai,<sup>b</sup> Dongsheng Geng,<sup>a</sup> Mohammad Norouzi Banis,<sup>a</sup> Ruying Li,<sup>a</sup> and Xueliang Sun<sup>a,\*\*,z</sup>

<sup>a</sup>Department of Mechanical and Materials Engineering, Faculty of Engineering, The University of Western Ontario, London, Ontario N6A 5B7 Canada

<sup>b</sup>General Motors R&D Center, Warren, Michigan 48090-9055, USA

This paper reports facile and cost effective methods for fabricating MoS<sub>2</sub> nanosheets and for assembling layered MoS<sub>2</sub>-graphene nanocomposites. The MoS<sub>2</sub> nanosheets were obtained by ultrasonically commercial MoS<sub>2</sub> powder in N-methyl-pyrrolidinone (NMP). The MoS<sub>2</sub>-graphene nanocomposites were assembled by the vacuum assisted filtration of a mixture of the MoS<sub>2</sub> nanosheets and graphene nanosheets suspended in NMP and water, respectively. In the nanocomposites, the MoS<sub>2</sub> nanosheets are dispersed between the graphene nanosheets, and vice versa. When used as anodes for LIBs, the MoS<sub>2</sub> nanosheets greatly outperform the MoS<sub>2</sub> powder; however, they still suffer severe capacity deterioration due to the poor electric conductivity and the obvious structural failure. Excellent performances were observed in the MoS<sub>2</sub>-graphene nanocomposites. For the 60Mo-80GN sample, the reversible capacities are held stably at ~650, ~550 and ~500 mAh g<sup>-1</sup> at 500, 1000 and 20000 mA g<sup>-1</sup>, respectively. It is concluded that for the MoS<sub>2</sub>-graphene nanocomposites, MoS<sub>2</sub> is the key component accommodating Li ions, and graphene improves the electric conductivity and maintains the structural stability for the MoS<sub>2</sub> nanosheets. These findings prove that ultrasonication combined with the vacuum assisted filtration is a scale-up approach to fabricate MoS<sub>2</sub>-graphene based layered nanocomposites with excellent Li storage capacity.

© 2013 The Electrochemical Society. [DOI: 10.1149/2.007310jss] All rights reserved.

Manuscript submitted July 1, 2013; revised manuscript received August 5, 2013. Published August 14, 2013. *This paper is part of the JSS Focus Issue on Nanocarbons for Energy Harvesting and Storage.*

A critical and challenging topic within materials research is the design and the synthesis of novel materials for lithium ion batteries (LIBs) with potential application to electric vehicles. Among potential anode materials is MoS<sub>2</sub> which is drawing increasing interest rapidly due to its high lithium storage capacity (~1000 mAh g<sup>-1</sup>).<sup>1-7</sup> Intrinsically, MoS<sub>2</sub> is a layered sulfide having the analogous structure of graphene. This structure is composed of three stacked atom layers (S-Mo-S) held together by van der Waals forces.<sup>8,9</sup> The weak interaction between MoS<sub>2</sub> layers was supposed to allow Li ions to diffuse easily. The battery performance of MoS<sub>2</sub> is highly dependent on its particle size and morphology.<sup>6</sup> Micro-scaled MoS<sub>2</sub> can offer initial reversible capacities over 600 mAh g<sup>-1</sup>,<sup>1,6</sup> which, however, decline quickly in the following charge-discharge cycles. One of the solutions for this is to fabricate nano-MoS<sub>2</sub> (usually nanosheets resulting from its layered structure), which is expected to enhance the MoS<sub>2</sub>-electrolyte contact and reduce the diffusing distance of Li in the interior of the electrode and consequently, improve Li storage capacity. Many methods have been proposed to synthesize and fabricate MoS<sub>2</sub> nanosheets, such as mechanical exfoliation of lithiated bulk MoS<sub>2</sub> in water,<sup>6,8</sup> chemical vapor deposition,<sup>10</sup> hydrothermal reaction using various kinds of precursors,<sup>1,4</sup> ball milling followed by high-temperature annealing, etc.<sup>11,12</sup> High quality MoS<sub>2</sub> nanosheets with improved battery performances were thus produced, e.g., >800 mAh g<sup>-1</sup> reported by Xiao, et al.<sup>6</sup> However, these methods usually involve either high cost chemicals or chemical reactions under harsh conditions and more importantly, the yield is low and their practical applications are thus limited.

Recently, Coleman, et al., reported that by choosing a suitable solvent, MoS<sub>2</sub> nanosheets can be easily obtained by ultrasonically MoS<sub>2</sub> powder, making massive production of MoS<sub>2</sub> nanosheets at low cost possible.<sup>13</sup> But, this does not solve all the problems with the application of MoS<sub>2</sub> in LIBs. The performances of MoS<sub>2</sub> nanosheets used as LIB anodes are not satisfying due to their limited electric conductivity, and introduction of a conductive component is indispensable to obtain and maintain high performances of the MoS<sub>2</sub> nanosheets.

This has evoked extensive research interest in designing and fabricating novel MoS<sub>2</sub>-carbon hybrid nanocomposites with excellent Li storage capacities,<sup>1-5</sup> including incorporation of the MoS<sub>2</sub> nanosheets into polymers,<sup>6</sup> hydrothermal based reactions,<sup>4</sup> biomolecular-assisted synthesis.<sup>1</sup> Nevertheless, like the most approaches for the synthesis of MoS<sub>2</sub> nanosheets, these approaches also employ expensive precursors and involve harsh reactions. The yield is low; the cost is high and as such, the possibility of commercialization is yet seen. Moreover, in the existing studies, the intrinsic factors that mediate the battery performances of the MoS<sub>2</sub>-carbon nanocomposites remain unanswered. Both carbon and MoS<sub>2</sub> in the nanocomposites evolve from chemical processes with one or more complicated precursors, as a consequence, the morphologies of MoS<sub>2</sub> and carbon is hard to be distinguished (notice the two kinds of nanosheets are ultrathin and are structurally analogous).<sup>14</sup> The MoS<sub>2</sub>-carbon interactions, i.e., how is MoS<sub>2</sub> grown onto carbon sheets, or vice versa, have not been well explained, either. Synergic effect is just a hypothesis.<sup>1</sup> These questions are able to be answered if MoS<sub>2</sub>-carbon nanocomposites are made of MoS<sub>2</sub> nanosheets and carbon nanosheets through a physical process directly.

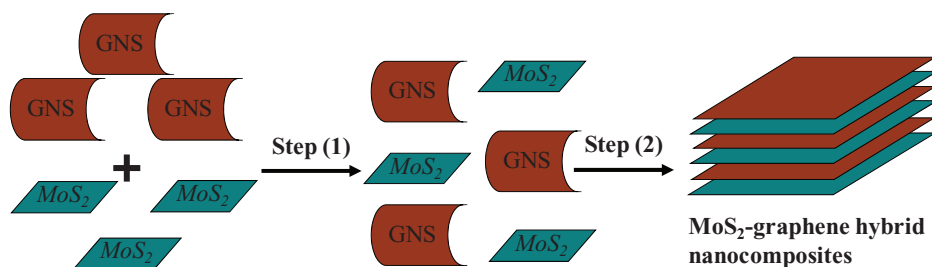
Graphene is an atomic layer of graphite.<sup>15</sup> Ever since the chemical exfoliation of graphite oxide (large scale production) succeeded, graphene has been considered a promising electrode material for LIBs due to its unique features such as high surface area, super electric conductivity and high tensile strength, etc.<sup>16-19</sup> Uniform graphene nanosheets (single layer or several layers) can be obtained simply by ultrasonically graphite oxide in water,<sup>20</sup> offering a new platform for facile fabricating carbon based materials. So far, various types of graphene-based materials have been reported,<sup>21-26</sup> some of which also exhibit intriguing electrochemical properties when used as electrode materials for LIBs.<sup>21,22,25,26</sup> On the other hand, the structural analog between graphene and MoS<sub>2</sub> nanosheets suggests an easy route to fabricate layered MoS<sub>2</sub>-graphene nanocomposites, i.e., layer by layer assembly, which is yet reported.

In this paper, we developed facile methods for fabricating MoS<sub>2</sub> nanosheets and for assembling layered MoS<sub>2</sub>-graphene nanocomposites and investigated their electrochemical properties as anodes for LIBs, focusing on the following key questions: (1) is there a strong interaction between MoS<sub>2</sub> and graphene nanosheets in the

\*Electrochemical Society Student Member.

\*\*Electrochemical Society Active Member.

<sup>z</sup>E-mail: xsun9@uwo.ca



Step (1): Mixed under the assistance of ultrasonication

Step (2): Filtration under the assistance of vacuum

**Figure 1.** Schematic diagram of assembling the MoS<sub>2</sub>-graphene nanocomposites by the vacuum-assisted filtration of MoS<sub>2</sub> and graphene nanosheets dispersed in NMP and water, respectively.

nanocomposites? (2) what are the roles of the two components in Li storage? (3) is there a synergic effect between the two composites for Li storage and what is it?

### Experimental

**Materials fabrication.—Graphene and MoS<sub>2</sub> nanosheets.**—Graphite oxide was synthesized using modified Hummers method with KMnO<sub>4</sub>, NaNO<sub>3</sub>, and H<sub>2</sub>SO<sub>4</sub> as the oxidants.<sup>27</sup> As-synthesized graphite oxide was dispersed in deionized water at a concentration of 0.5 mg ml<sup>-1</sup>, and was then exfoliated by ultrasonication for 1 h. The obtained dispersion was centrifuged at 5000 rpm for 15 min. The solution was then harvested for further use. MoS<sub>2</sub> nanosheets were fabricated by exfoliation of commercial MoS<sub>2</sub> powder. 0.5 g MoS<sub>2</sub> powder was dispersed in 100 mL NMP and was then ultrasonicated for 12 h. The suspension was centrifuged at 2000 rpm for 40 min. The upper part 2/3 dispersion was harvested for further use.

To assure the absolute amounts of MoS<sub>2</sub> and graphene in the final nanocomposites are controllable, about 500 mL MoS<sub>2</sub> and graphene suspensions were pre-prepared for use, respectively.

**Graphene-MoS<sub>2</sub> nanocomposites.**—Graphene nanosheets and MoS<sub>2</sub> nanosheets suspended in water and in NMP, respectively, were mixed at a requisite ratio. The mixture was then ultrasonicated for 1 h so as to get a homogeneous mixture, and was then filtrated under the assistant of vacuum through an Anodisc membrane filter (47 mm diameter, 0.2 μm pore size; Whatman). The solid product was harvested and dried in air for 24 h at ~100°C. The whole procedure is schematically shown in Fig. 1. Before spectroscopic and electrochemical characterization, the samples were mildly annealed in Ar-H<sub>2</sub> (10% H<sub>2</sub>) atmosphere at 800°C for 2 h for additional deoxygenation of graphene. Since it is hard to define the absolute amounts of the nanosheets in solvents, in this paper, the ratios of graphene and MoS<sub>2</sub> in the composites were expressed in term of volume. For example, 60MoS<sub>2</sub>-80GN corresponds to the sample containing 80 mL graphene nanosheets in water and 60 mL MoS<sub>2</sub> nanosheets in NMP, respectively.

**Materials characterization.**—The morphologies of nanocomposites were checked using a field emission scanning electronic microscope (Hitachi S-4800), transmission electronic microscope (Philips CM10), and high resolution TEM (JEOL 2010 FEG). Powder X-ray diffraction (XRD) patterns were recorded by Rigaku RU-200BVH diffractometer employing a Co-Kα source ( $\gamma = 1.7892 \text{ \AA}$ ). Raman spectra were obtained using a HORIBA Scientific LabRAM HR Raman spectrometer system equipped with a 532.4 nm laser as the exciting radiation. The system is also equipped with an optical microscope so as to give rise to confocal signals. To obtain charge-discharge profiles and cycle performance data, working electrodes were prepared by slurry casting onto a Cu foil as a current collector. The slurry contained the synthesized sample (90 wt% on dry solid basis), polyvinylidene fluoride binder (10 wt% on dry solid basis) and carbon conductor (10 wt%) in NMP solvent. The electrodes were dried in a vacuum oven at 100°C overnight. A lithium foil was used as a counter electrode. Paper based MoS<sub>2</sub>-graphene nanocomposite was used as anode

directly, i.e., current collector and binder are not used. Electrolyte was composed of 1 M LiPF<sub>6</sub> salt dissolved in a solution consisting ethylene carbonate, diethyl carbonate, ethyl methyl carbonate (1:1:1 in volume). Charge-discharge characteristics were tested galvanostatically in a voltage range of 0.01–3.0 V (vs. Li<sup>+</sup>/Li) at a desired current density using an Arbin BT-2000 Battery Test System. Cyclic voltammetry (CV) tests were performed on a versatile multichannel potentiostat 3/Z (VMP3) at a scan rate of 0.1 mV.s<sup>-1</sup> over a potential range of 0.01–3.0 V (vs. Li<sup>+</sup>/Li).

### Results and Discussion

**Characterization of the MoS<sub>2</sub> nanosheets and the MoS<sub>2</sub>-graphene nanocomposites.**—The GNS from mechanical exfoliation of graphite oxide have been characterized in detail in our previous studies.<sup>28</sup> The GNS are usually ultrathin and are easily to restack to form graphene papers when filtrated. A typical TEM image of the GNS is shown in Fig. S1(a) as an example. The crystal structure of the nanosheets resulting from ultrasonication MoS<sub>2</sub> powder in NMP is determined using XRD, Raman spectrum and HRTEM. Figure 2a shows the XRD patterns of the MoS<sub>2</sub> powder and the 100MoS<sub>2</sub>-20GN sample. The 100MoS<sub>2</sub>-20GN pattern is presented because of its relatively higher MoS<sub>2</sub> content and therefore, the information on the crystal structure of the MoS<sub>2</sub> nanosheets and whether the crystal structure is preserved in the nanocomposites is conveyed, simultaneously. The 100MoS<sub>2</sub>-20GN pattern is similar to that of the MoS<sub>2</sub> powder. The peaks appearing in the powder MoS<sub>2</sub> pattern are also observed in the 100MoS<sub>2</sub>-20GN pattern, i.e., at  $2\theta = 16.7, 33.7, 46.2, 51.7$  and  $58.5^\circ$ , respectively. Among them, the peak at  $2\theta = 16.7^\circ$  is corresponding to the (002) reflection, a typical feature of the layered structure of MoS<sub>2</sub>.<sup>1</sup> The broad peak at  $2\theta = 30.7^\circ$  in the 100MoS<sub>2</sub>-20GN pattern is corresponding to the diffraction of the graphene nanosheets.<sup>29</sup> When MoS<sub>2</sub> nanosheets stack with graphene nanosheets layer by layer forming 2-dimensional structure, some of the typical MoS<sub>2</sub> peak will not be accessed by X-ray because the special orientation of the sheets (e.g.,  $38.1, 39.1$  and  $41.9$  in the MoS<sub>2</sub> pattern). That is why some diffraction peaks of MoS<sub>2</sub> are not observed in the nanocompositions.

The Raman spectra of the MoS<sub>2</sub> powder and the MoS<sub>2</sub> nanosheets are shown in Fig. 2b. There are no evident differences between the two spectra. For both, two predominant peaks appear at  $\sim 375 \text{ cm}^{-1}$  (E<sub>2g</sub>) and  $\sim 404 \text{ cm}^{-1}$  (A<sub>1g</sub>), respectively, which correspond to the typical vibrations of the Mo-S atoms in the  $\beta$ -phase MoS<sub>2</sub> (2H-MoS<sub>2</sub>).<sup>30,31</sup> The morphology of the MoS<sub>2</sub> nanosheets is characterized using SEM and TEM and is shown in Fig. 3. The average sizes of the MoS<sub>2</sub> nanosheets are  $\leq 500 \text{ nm}$ , as indicated by the SEM image in Fig. 3a. TEM image in Fig. 3b clearly shows that the nanosheets are very thin and the thickness is not uniform as some parts have more layers of MoS<sub>2</sub>. This probably results from restacking of the nanosheets upon solvent is removed. The top view of the HRTEM image (Fig. 3c) shows typical hexagonal structure formed by Mo and S atoms. The layer distance is  $\sim 0.65 \text{ nm}$  (Fig. 3d), which is consistent with other studies.<sup>1,6</sup> Based on the XRD, Raman and microscopic characterizations, it is reasonable to conclude that mechanical exfoliation and

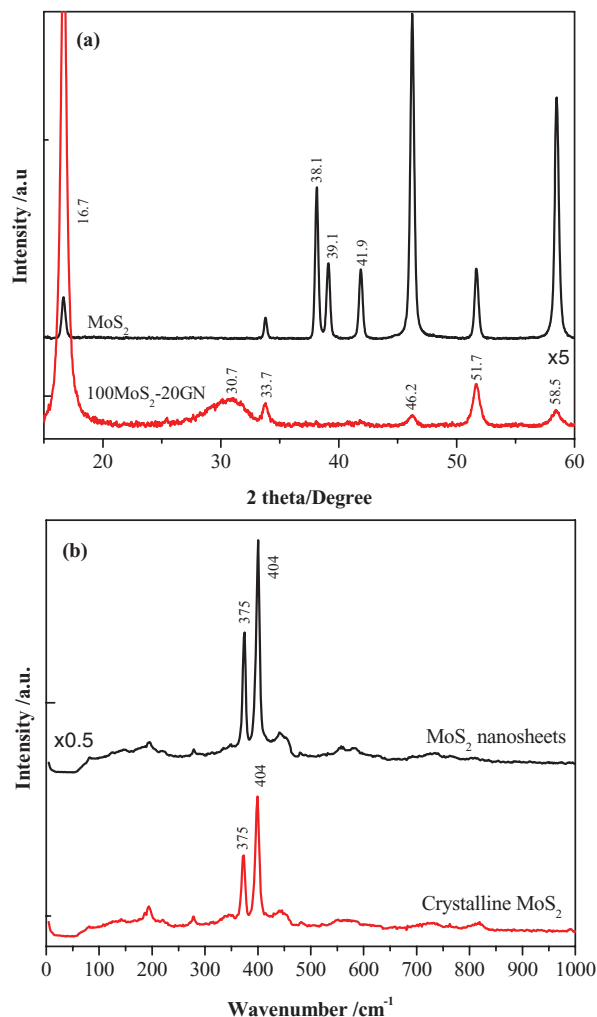


**Figure 2.** (a) XRD patterns of the commercial  $\text{MoS}_2$  powder and the  $100\text{MoS}_2$ -20GN composite; (b) Raman spectra of the  $\text{MoS}_2$  nanosheets and the commercial  $\text{MoS}_2$  powder.

hybridization with graphene does not change the crystal structure of  $\text{MoS}_2$ , and the layered structure is preserved.

It is a fact that during the process of filtration, both kinds of nanosheets, due to their two-dimension structures, stack together to form layered structure, i.e., macroscopically, thin films. The thickness of the film depends on how much solution was filtrated. The morphology of the  $60\text{MoS}_2$ -80GN sample is shown in Fig. 3. SEM image of the cross section of the sample indicates that the film thickness is  $\sim 15 \mu\text{m}$  (Fig. 3e). In the film, the  $\text{MoS}_2$  and the graphene nanosheets are aligned with their surface parallel to the film surface, and the  $\text{MoS}_2$  nanosheets are dispersed between the graphene sheets, and vice versa (Fig. 3f). This configuration is also manifested by the surface morphology of the sample (Fig. S1(b)). Distribution of the  $\text{MoS}_2$  and the graphene nanosheets was also characterized using EDX mapping. As shown in Fig. S2(a)-(d), the three composite elements, Mo, S and C are homogeneously distributed in the sample. It can thus follow that ultrasound-assisted mixing followed by the vacuum-assisted filtration is an effective approach to obtain the nanocomposites with  $\text{MoS}_2$  and graphene nanosheets uniformly mixed. Table I tabulates the contents of various elements presenting in the  $60\text{MoS}_2$ -80GN and  $100\text{MoS}_2$ -20GN samples, which are calculated according to the EDX mapping on the sample surfaces. Obviously, more graphene is present in the  $60\text{MoS}_2$ -80GN sample.

To get further insight of the distribution of the  $\text{MoS}_2$  and graphene nanosheets in the composites, the paper based nanocomposites were

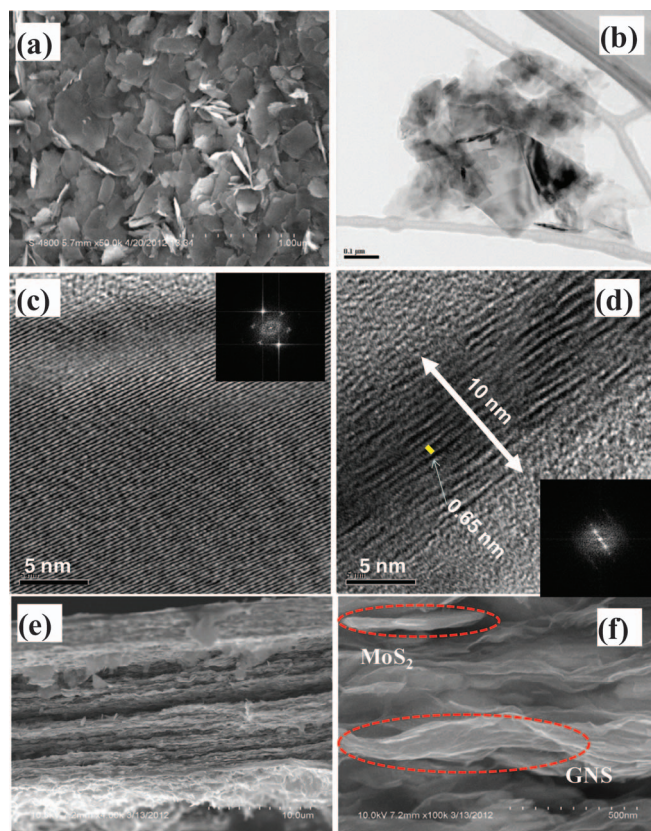


**Figure 3.** Electronic microscope images of the  $\text{MoS}_2$  nanosheets and the  $60\text{MoS}_2$ -80GN nanocomposites: (a) SEM image of the  $\text{MoS}_2$  nanosheets; (b) TEM image of  $\text{MoS}_2$  nanosheets; (c) HRTEM image of surface of the  $\text{MoS}_2$  nanosheets; (d) HRTEM image showing the thickness of the nanosheets; (e) lower magnification of the  $60\text{MoS}_2$ -80GN nanocomposite; (f) higher magnification of the  $60\text{MoS}_2$ -80GN nanocomposite.

ground and characterized using Raman. Before grind, i.e., the paper, the two typical  $\text{MoS}_2$  peaks remain considerable intensities in the  $100\text{MoS}_2$ -20GN spectrum, and are obviously stronger than those of graphene ( $1348 \text{ cm}^{-1}$  (D band) and  $1596 \text{ cm}^{-1}$  (G band)); in contrast, they are not observable in the  $60\text{MoS}_2$ -80GN spectrum, as shown in Fig. 4. This suggests that the  $\text{MoS}_2$  nanosheets are wrapped with the GNS and are not accessible to the laser at higher graphene content. Notice there are more GNS in the  $60\text{MoS}_2$ -80GN sample and the size of GNS can be several  $\mu\text{m}$ . See Fig. S1(a). After grind, i.e., the paper was converted into  $\mu\text{m}$ -sized irregular particles (Fig. S3), the peaks of the  $\text{MoS}_2$  nanosheets are enhanced dramatically, particularly, the peaks in the  $60\text{MoS}_2$ -80GN spectrum. Table II lists the ratios of the  $\text{MoS}_2$  peak ( $404 \text{ cm}^{-1}$ ) to the graphene peak ( $1596 \text{ cm}^{-1}$ ). Obviously, the  $\text{MoS}_2$  peaks are stronger than those of the graphene in both samples. This, semi-quantitatively, confirms that reducing the particle size of the  $\text{MoS}_2$ -graphene nanocomposites

**Table I.** The contents of the elements in the  $\text{MoS}_2$ -GN samples, estimated on the base of the EDX quantization.

| Sample                  | Element content (%) |         |          |           |             |
|-------------------------|---------------------|---------|----------|-----------|-------------|
|                         | C                   | O       | Mo       | S         | C/Mo ratio* |
| $60\text{MoS}_2$ -80GN  | 69.6/85.6           | 8.3/7.1 | 11.3/1.7 | 10.8/5.1  | 6.2/50.4    |
| $100\text{MoS}_2$ -20GN | 49.7/77.3           | 4.3/5.1 | 22.9/4.5 | 22.9/13.3 | 2.2/17.2    |

\*In this table, the element contents are expressed as weight percent and atomic percent, e.g., for C/Mo ratios, a 6.2 corresponds to weight ratio while 50.4 corresponds to atomic ratio.

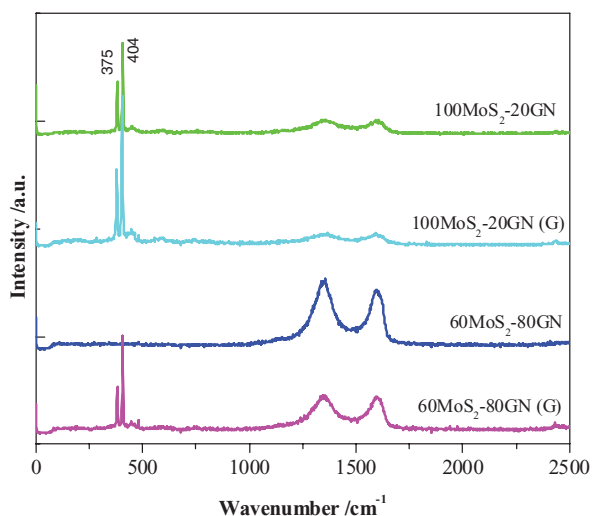


**Figure 4.** Raman spectra of the MoS<sub>2</sub>-graphene nanocomposites.

enables more MoS<sub>2</sub> to be accessible. This is one of the key issues that mediate the battery performances of the MoS<sub>2</sub>-graphene nanocomposites and will be further addressed later. Meanwhile, it should be mentioned that for the MoS<sub>2</sub>-graphene spectra, there are no new peaks observed, and the peaks of MoS<sub>2</sub> and graphene do not change evidently. This, combined with the XRD results, suggests there are not discernable chemical reactions between MoS<sub>2</sub> and graphene following annealing at 800°C, and MoS<sub>2</sub> and graphene only physically stack together.

*Electrochemical properties of the MoS<sub>2</sub>-graphene nanocomposites.*—The CV curves were obtained using the MoS<sub>2</sub> containing materials as electrodes in 1.0 M LiPF<sub>6</sub> and with lithium sheet as the counter and reference electrodes. Figure 5 shows the CV curves of the MoS<sub>2</sub> nanosheets and the 60MoS<sub>2</sub>-80GN nanocomposites. The curves of the MoS<sub>2</sub> powder are shown in Fig. S4. Some interesting features are observed for the electrochemical behaviors of the samples:

- Basically, the curves do not vary greatly with the morphology of MoS<sub>2</sub> and the composition of the MoS<sub>2</sub>-graphene nanocomposites. For the 60MoS<sub>2</sub>-80GN curves, as an example, on the first cycle, two predominant peaks appear at ~1.07 V and ~0.49 V in the discharge process. The ~1.07 V peak can be attributed to the coordination of Mo by six S atoms (MoS<sub>6</sub>) changing from trigonal prisms to octahedral in the MoS<sub>2</sub> structure as lithium ions intercalate into MoS<sub>2</sub>.<sup>1,32–36</sup> The 0.49 V peak is attributed to the conversion reaction process MoS<sub>2</sub>+4Li→Mo+2Li<sub>2</sub>S.<sup>1,32–36</sup> The peak appearing at ~2.3 V in the charge process corresponds to delithiation. In the following cycles, the cathode peaks (~0.49 and ~1.07 V) are diminished significantly, but the anode peak (~2.3 V) still remains considerably high intensities. Moreover, a new peak appears at ~1.96 V in the discharge process, which can reasonably be attributed to lithiation.<sup>32</sup> Following these features, it can be concluded that for the 60MoS<sub>2</sub>-80GN sample,

**Table II.** The intensity ratios of the MoS<sub>2</sub> peak (404 cm<sup>-1</sup>) to the graphene peak (1596 cm<sup>-1</sup>) for the MoS<sub>2</sub>-GN samples.

| Sample                    | Ratios of the MoS <sub>2</sub> peak to the graphene peak (a.u.) |        |
|---------------------------|---|--------|
|                           | As synthesized  | Ground |
| 60MoS <sub>2</sub> -80GN  | –   | 2.7    |
| 100MoS <sub>2</sub> -20GN | 7.6   | 12.3   |

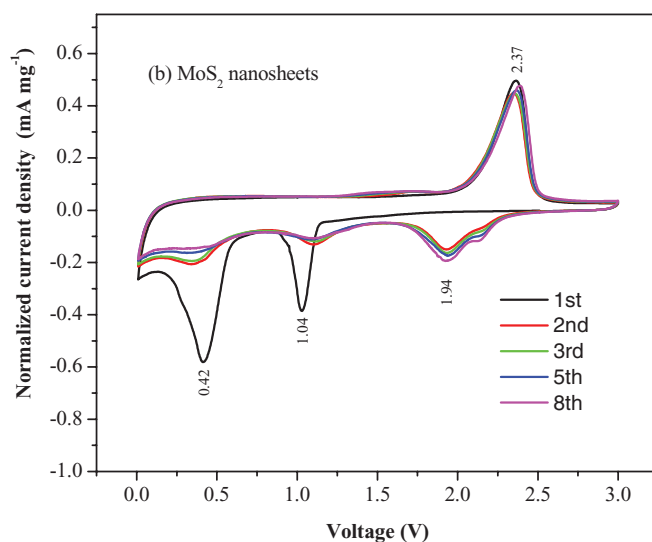
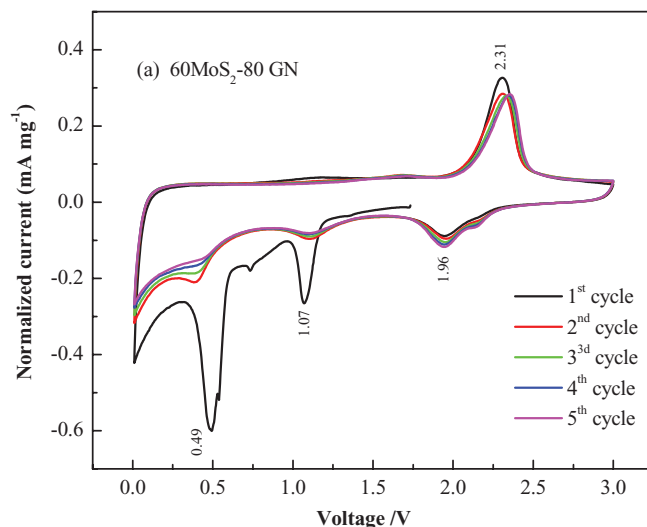


**Figure 5.** CV curves of the MoS<sub>2</sub>-containing samples: (a) the MoS<sub>2</sub> nanosheets; (b) the 60MoS<sub>2</sub>-80GN nanocomposites.

Li-MoS<sub>2</sub> interaction is a leading process. It should be mentioned the electrochemical processes of lithium-MoS<sub>2</sub> interactions are very complicated, because the processes are highly dependent on samples, i.e., the particle size of MoS<sub>2</sub>, the carbon component and the methods for materials synthesis, etc.<sup>32–36</sup> The CV curves may differ slightly from different research groups, but the assignment of the typical peaks (~0.41, ~1.07, ~1.94 and ~2.31 V) is very defined.

- There are discernable differences among the curves of the three samples. For the powder MoS<sub>2</sub> curves, the ~2.3 V peak loses intensity steadily with cycles, suggesting that the electrochemical performance is deteriorating. For the 60MoS<sub>2</sub>-80GN curves, the peak intensity in the second cycle is only slightly lower than that on the first cycle, and remains almost unchanged in the following cycles. Interestingly, for the MoS<sub>2</sub> nanosheets, the intensity of the same peak does not change for all in the first ten cycles. Accordingly, it can be suggested that the electrochemical performances of the MoS<sub>2</sub> nanosheets are much better than that of the MoS<sub>2</sub> powder.

Battery performances of the MoS<sub>2</sub> containing materials were tested in coin cells. Since the performances vary dramatically, the current densities are varied so that the performance change following charge-discharge cycles can be clearly manifested. As shown in Fig. 6a, the

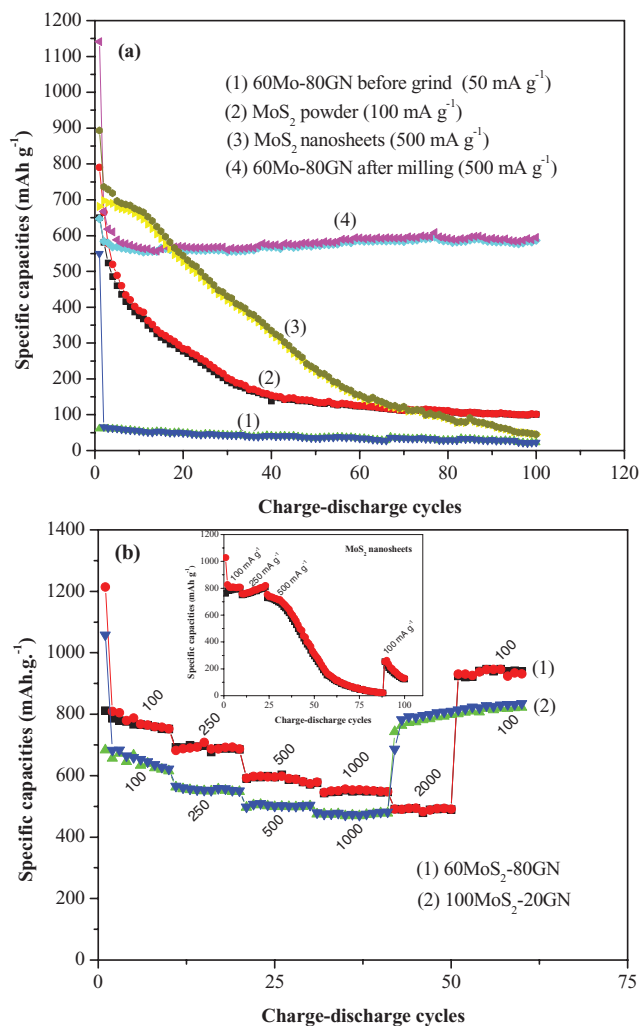


**Figure 6.** Electrochemical performances of the MoS<sub>2</sub>-containing samples.

MoS<sub>2</sub> powder offers initial reversible specific capacities of  $\sim 660$  mAh g<sup>-1</sup> at 100 mA g<sup>-1</sup>, which, however, decline very rapidly and remain only  $\sim 100$  mAh g<sup>-1</sup> in the 100<sup>th</sup> cycle. In contrast, the performances of the MoS<sub>2</sub> nanosheets are much better. At 500 mA g<sup>-1</sup>, the initial reversible specific capacities of  $\sim 750$  mAh g<sup>-1</sup> were obtained, which decrease slightly in the first 15 cycles. Obviously, reduction of particle size facilitates Li-MoS<sub>2</sub> interaction, improving electrochemical performance of MoS<sub>2</sub>. But it does not relieve the drawback of the poor electric conductivity of MoS<sub>2</sub> as well as high volume change with cycles. As a result, the decline proceeds at a much rapider pace after 15 cycles, and only  $\sim 50$  mAh g<sup>-1</sup> capacity remains in the 100<sup>th</sup> cycles. The 60MoS<sub>2</sub>-80GN sample was tested before and after grind. For the paper based sample, i.e., before grind, the reversible specific capacities are only  $\sim 60$  mAh g<sup>-1</sup> at 50 mA g<sup>-1</sup> throughout the charge-discharge cycles. On the other hand, for the powder based sample, i.e., after grind, the sample exhibits the best performances among the MoS<sub>2</sub> containing samples. The initial capacities are  $\sim 700$  mAh g<sup>-1</sup> at 500 mA g<sup>-1</sup>, which decrease to  $\sim 600$  mAh g<sup>-1</sup> after 10 cycles. The capacities remain rising at a slow pace in the following cycles. This, combined with Raman spectra in Fig. 4, confirms that reducing particle size provides much more channels for Li ion to diffuse in and out of the MoS<sub>2</sub> nanosheets in the nanocomposites, improving Li-MoS<sub>2</sub> interaction and consequently the lithium storage capacities of the nanocomposites.

Rate cycling behaviors of the MoS<sub>2</sub> based samples were also investigated so as to further interrogate the relationship between the particle sizes and the electrochemical performances. As shown in Fig. 6b, the

MoS<sub>2</sub>-graphene samples exhibit much better performances than the nanosheets do. For the nanosheets, the specific capacities do not vary greatly at 100 and 250 mA g<sup>-1</sup>, holding  $\sim 800$  mAh g<sup>-1</sup> in the cycles adopted in this study. However, when the current density is increased to 500 mA g<sup>-1</sup>, the capacities decline abruptly to  $\sim 20$  mAh g<sup>-1</sup> after 75 cycles, and only 250 mAh g<sup>-1</sup> was regained as the current density is re-set to 100 mA g<sup>-1</sup> from 500 mA g<sup>-1</sup> (see the inserted panel in Fig. 6b). The capacities decrease to almost zero again in the following tens of cycles. In contrast, at 500 mA g<sup>-1</sup>, the 60MoS<sub>2</sub>-80GN sample exhibits constant capacities of  $\sim 600$  mAh g<sup>-1</sup>, which decrease to  $\sim 550$  and  $\sim 500$  mAh g<sup>-1</sup>, at 1000 and 2000 mA g<sup>-1</sup>, respectively. More importantly, when the current density was re-set to 100 from 2000 mA g<sup>-1</sup>, the capacities were abruptly raised to  $\sim 950$  mAh g<sup>-1</sup>, which remain rising steadily. These are almost 300 mAh g<sup>-1</sup> higher than those obtained at the same current density in the beginning of the cycles. This phenomenon was also observed in other systems and further corroborates the particle size effect (*to be addressed in detail later*).<sup>37,38</sup> To articulate the relationship between the battery performance and the MoS<sub>2</sub>/graphene ratio, the rate cycling behavior of the 100MoS<sub>2</sub>-20GN sample, which has a higher Mo/C ratio (see Table I), was also tested. As also shown in Fig. 6b, the rate cycling behavior is similar to that of the 60MoS<sub>2</sub>-80GN sample, with exception that the specific capacities are slightly lower than those of the 60MoS<sub>2</sub>-80GN sample at an equal current density. Nevertheless, the capacities are still much higher than those of the MoS<sub>2</sub> nanosheets. This confirms that graphene is also crucial to deliver and maintain higher capacities for the MoS<sub>2</sub>-graphene nanocomposites.

Overall, following the spectroscopic and electrochemical characterizations, the questions put forward in the beginning of this paper could be answered or articulated. SEM characterization manifests that the MoS<sub>2</sub> nanosheets and the graphene nanosheets closely stack together following filtration; however, a combination of the Raman and XRD characterization proves that there are no strong interactions between MoS<sub>2</sub> and graphene that result in formation of new species. Moreover, CV characterization indicates that the Li-MoS<sub>2</sub> interaction is a predominant electrochemical process for the MoS<sub>2</sub>-graphene nanocomposite electrode. Most of previous studies prove that the reversible Li storage capacities of graphene following extended charge-discharge cycles (>50 cycles) are only between 300 and 400 mAh g<sup>-1</sup> at a current density of 100 mA g<sup>-1</sup> or lower,<sup>39,40</sup> which are much lower than those of the MoS<sub>2</sub> nanosheets and the present MoS<sub>2</sub>-graphene nanocomposites. Thus, it is reasonable to conclude that for the MoS<sub>2</sub>-graphene nanocomposites, MoS<sub>2</sub> is the key component that accommodates Li.

*Characterization of the samples after test.*— To reliably explore the role of graphene in the MoS<sub>2</sub>-graphene nanocomposites, particularly, if there is a synergic effect, the MoS<sub>2</sub> nanosheets and the 60MoS<sub>2</sub>-80GN nanocomposite were characterized using SEM after electrochemical tests. Figure 7 compares the images of the electrode materials before and after test. The morphology changes significantly after charge-discharge cycles. For the MoS<sub>2</sub> nanosheets electrode, the nanosheets are indistinguishable after repeated lithiation-delithiation; instead, many particles with sizes <20 nm are found (Fig. 7b). This indicates that the MoS<sub>2</sub> nanosheets undergo severe pulverization and as a consequence, the bulk materials are disintegrated (mechanical failure), leading to the disconnection of some particles from the conductive carbon or current collector, a main reason for the capacity deterioration of the MoS<sub>2</sub> nanosheets. For the 60MoS<sub>2</sub>-80GN nanocomposite, the image is still composed of particles with sizes in sub- $\mu$ m scale (Fig. S5). The magnified image (Fig. 7d) shows that the particles remain highly integrated whereas some pores are created; in other words, the electrode materials mostly remain integrated. Obviously, the presence of graphene effectively maintains the structural stability for the MoS<sub>2</sub> nanosheets. This, combined with its super electric conductivity, accounts for the role of graphene in MoS<sub>2</sub>-graphene nanocomposite.

It is worth emphasizing that particle size is another important factor in the battery performances of the MoS<sub>2</sub>-graphene nanocomposites,

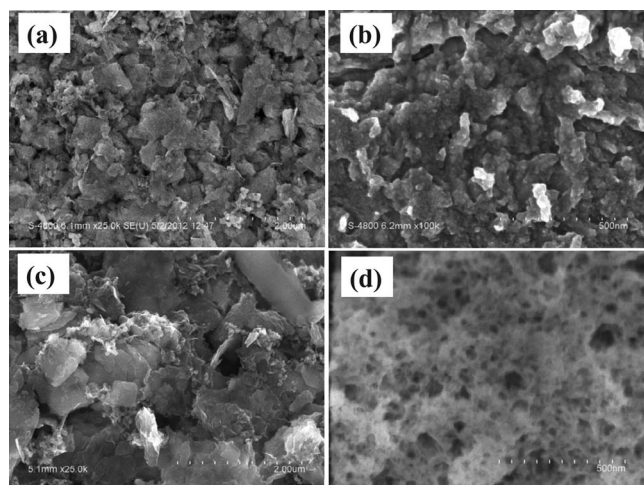


**Figure 7.** SEM images of the MoS<sub>2</sub> nanosheets pasted on current collector before (a) and after (b) test; the 60MoS<sub>2</sub>-80GN nanocomposites pasted on current collector before (c) and after (b) test.

which is also mediated by graphene. For graphene, the cross-plane diffusion of Li ions is forbidden. As such, in the MoS<sub>2</sub>-graphene nanocomposites, lithium diffusion in MoS<sub>2</sub> nanosheets mostly proceeds in the direction along the nanosheet surfaces, since the MoS<sub>2</sub> nanosheets are wrapped with graphene nanosheets. This is the reason why the paper based 60MoS<sub>2</sub>-80GN nanocomposite only presents reversible capacities of ~60 mAh g<sup>-1</sup> at a very low current density, i.e., 50 mA g<sup>-1</sup> (in Fig. 6a). Such a fact also explains the rate cycling behavior of the MoS<sub>2</sub>-graphene nanocomposites in Fig. 6b, which has shown that the capacities of the MoS<sub>2</sub>-graphene nanocomposites are lower than those of the MoS<sub>2</sub> nanosheets at 100 and 200 mA g<sup>-1</sup>. Nevertheless, the graphene-induced size effect can be easily released in two ways. First, reducing the thickness of nanocomposites when assembling; and second, ball milling the nanocomposites after assembly. This has been addressed in other researches and is not the main focus of this paper.

In summary, in this paper, we reported facile methods for fabricating MoS<sub>2</sub> nanosheets and for assembling MoS<sub>2</sub>-graphene nanosheets. This approach offers several advantages over other methods. First, exfoliating commercial MoS<sub>2</sub> powder in NMP means purification of the MoS<sub>2</sub> nanosheets and final products is not necessary since NMP is a standard solvent for preparing electrode slurry and as such; second, NMP can be reusable for another exfoliation, significantly reducing the cost; third, this method allows massive production and has a high potential to be scaled up.

### Conclusions

Mechanical exfoliation of MoS<sub>2</sub> powder in NMP by ultrasonication is a facile and cost-effective method for obtaining MoS<sub>2</sub> nanosheets with thickness <20 nm. The resultant nanosheets exhibit better battery performances than MoS<sub>2</sub> powder does when used as anodes for lithium ion batteries. However, the nanosheets still suffer capacity deterioration during the extended charge-discharge cycles and hence; their practical application is yet seen. MoS<sub>2</sub>-graphene nanocomposites were fabricated through the vacuum-assisted filtration of a mixture of MoS<sub>2</sub> and graphene nanosheets suspended in suitable solvents. Images taken of the fabricated nanocomposites reveal that both kinds of nanosheets closely stack together and are aligned with their surface parallel to each other. The performances of the MoS<sub>2</sub>-graphene nanocomposites are much higher than that of MoS<sub>2</sub> nanosheets. The reversible capacities were held stably at ~650, ~550 and ~500 mAh g<sup>-1</sup> at 500, 1000 and 2000 mA g<sup>-1</sup>, respectively. It is concluded that

for the MoS<sub>2</sub>-graphene nanocomposites, MoS<sub>2</sub> is the key component that stores Li ions, and the presence of graphene improves the electric conductivity and structural stability of MoS<sub>2</sub> sheets. The findings in this paper provide a strong evidence that layer-by-layer assembly is a cost-effective method to massively fabricate graphene based nanocomposites with superior battery performances.

### Acknowledgments

This research was supported by Natural Science and Engineering Research Council of Canada (NSERC), General Motors of Canada, Canada Research Chair (CRC) Program, Ontario Research Fund (ORF) and the University of Western Ontario.

### References

1. K. Chang and W. X. Chen, *ACS Nano*, **5**, 4720 (2011).
2. C. Q. Feng, J. Ma, H. Li, R. Zeng, Z. P. Guo, and H. K. Liu, *Mater. Res. Bull.*, **44**, 1811 (2009).
3. H. Li, W. J. Li, L. Ma, W. X. Chen, and J. M. Wang, *J. Alloys Compd.*, **471**, 442 (2009).
4. H. Hwang, H. Kim, and J. Cho, *Nano Lett.*, **11**, 4826 (2011).
5. G. Du, Z. Guo, S. Wang, R. Zeng, Z. Chen, and H. Liu, *Chem. Comm.*, **46**, 1106 (2010).
6. J. Xiao, D. Choi, L. Cosimbescu, P. Koech, J. Liu, and J. P. Lemmon, *Chem. Mater.*, **22**, 4522 (2010).
7. S. J. Ding, J. S. Chen, and X. W. Lou, *Chem. A Eur.*, **17**, 13142 (2011).
8. H. S. S. Ramakrishna Matte, A. Gomathi, A. K. Manna, D. J. Late, R. Datta, S. K. Pati, and C. N. R. Rao, *Angew. Chem. Int. Ed.*, **49**, 4059 (2010).
9. R. Tenne, L. Margulis, M. Genut, and G. Hodes, *Nature*, **360**, 444 (1992).
10. N. Imanishi, K. Kanamura, and Z. Takehara, *J. Electrochem. Soc.*, **139**, 2082 (1992).
11. Z. Z. Wu, D. Z. Wang, X. Liang, and A. K. Sun, *J. Crystal Growth*, **312**, 1973 (2010).
12. Z. Z. Wu, D. Z. Wang, Y. Wang, and A. K. Sun, *Adv. Eng. Mater.*, **12**, 534 (2010).
13. J. N. Coleman, M. Lotya, A. O'Neill, and S. D. Bergin, etc. *Science*, **331**, 568 (2011).
14. K. Chang, D. Geng, X. Li, J. Yang, Y. Tang, M. Cai, R. Li, and X. Sun, *Adv. Energy Mater.*, **3**, 839 (2013).
15. K. S. Novoselov, A. K. Geim, S. V. Morozov, D. Jiang, Y. Zhang, S. V. Dubonos, I. V. Grigorieva, and A. A. Firsov, *Science*, **306**, 666 (2004).
16. X. Huang, X. Y. Qi, F. Boey, and H. Zhang, *Chem. Soc. Rev.*, **41**, 666 (2012).
17. D. A. C. Brownson, D. K. Kampouris, and C. E. Banks, *J. Power Sources*, **196**, 4873 (2011).
18. Y. Q. Sun, Q. Wu, and G. Q. Shi, *Energy Environ. Sci.*, **4**, 1113 (2011).
19. M. J. Allen, V. C. Tung, and R. B. Kaner, *Chem. Rev.*, **110**, 132 (2011).
20. D. A. Dikin, S. Stankovich, E. J. Zimney, R. D. Piner, G. H. B. Dommett, G. Evmenenko, S. T. Nguyen, and R. S. Ruoff, *Nature*, **448**, 457 (2007).
21. H. Q. Chen, M. B. Mueller, K. J. Gilmore, G. G. Wallace, and D. Li, *Adv. Mater.*, **20**, 3557 (2008).
22. J. K. Lee, K. B. Smith, C. M. Hayner, and H. H. Kung, *Chem. Comm.*, **46**, 2025 (2010).
23. Z. Li, Y. Mi, X. Liu, S. Liu, S. Yang, and J. Wang, *J. Mater. Chem.*, **21**, 14706 (2011).
24. J. Liang, Y. Xu, D. Sui, L. Zhang, Y. Huang, Y. Ma, F. Li, and Y. Chen, *J. Phys. Chem. C*, **114**, 17465 (2011).
25. H. Gwon, H. Kim, K. U. Seo, D. Lee, Y. C. Park, Y. S. Lee, B. T. Ahn, and K. Kang, *Energy Environ. Sci.*, **4**, 1277 (2011).
26. C. Wang, D. Li, C. O. Too, and G. G. Wallace, *Chem. Mater.*, **21**, 2604 (2008).
27. W. S. Hummers and R. E. Offeman, *J. Am. Chem. Soc.*, **80**, 1339 (1958).
28. Y. H. Hu, X. Li, D. Geng, R. Li, M. Cai, and X. L. Sun, *Electrochimica Acta*, **91**, 227 (2013).
29. G. Q. Wang, W. Xing, and S. P. Zhuo, *Electrochim Acta*, **66**, 151 (2012).
30. B. C. Windom, W. G. Sawyer, and D. W. Hahn, *Trib. Letts.*, **42**, 301 (2011).
31. C. Julien, T. Sekine, and M. Balkanski, *Solid State Ion.*, **48**, 225 (1991).
32. K. Bindumadhavan, S. K. Srivastava, and S. Mahanty, *Chem. Comm.*, **49**, 1823 (2013).
33. Q. Wang and J. Li, *J. Phys. Chem. C*, **111**, 1675 (2007).
34. G. D. Du, Z. P. Guo, S. Q. Wang, R. Zeng, Z. X. Chen, and H. K. Liu, *Chem. Comm.*, **45**, 1106 (2010).
35. L. Yang, S. Wang, J. Mao, J. Deng, Q. Gao, Y. Tang, and O. G. Schmidt, *Adv. Mater.*, **25**, 1190 (2013).
36. M. Wang, G. Li, H. Xu, Y. Qian, and J. Yang, *ACS Appl. Mater. Interfaces*, **5**, 1003 (2013).
37. J. Shen and R. Raj, *J. Power Source*, **196**, 5945 (2011).
38. W. H. Shin, H. M. Jeong, B. G. Kim, J. K. Kang, and J. W. Choi, *Nano Lett.*, **12**, 2283 (2012).
39. C. O. A. Caballero, and J. Morales, *Nanoscale*, **4**, 2083 (2012), and references therein.
40. X. F. Li, D. Geng, Y. Zhang, X. Meng, R. Li, and X. Sun, *Electrochem. Comm.*, **13**, 822 (2011).